



OPEN

# High-throughput image processing software for the study of nuclear architecture and gene expression

Adib Keikhosravi<sup>1</sup>, Faisal Almansour<sup>2,4,5</sup>, Christopher H. Bohrer<sup>3</sup>, Nadezda A. Fursova<sup>3</sup>, Krishnendu Guin<sup>2,5</sup>, Varun Sood<sup>2,3,5</sup>, Tom Misteli<sup>2</sup>, Daniel R. Larson<sup>3</sup> & Gianluca Pegoraro<sup>1</sup>✉

High-throughput imaging (HTI) generates complex imaging datasets from a large number of experimental perturbations. Commercial HTI software programs for image analysis workflows typically do not allow full customization and adoption of new image processing algorithms in the analysis modules. While open-source HTI analysis platforms provide individual modules in the workflow, like nuclei segmentation, spot detection, or cell tracking, they are often limited in integrating novel analysis modules or algorithms. Here, we introduce the High-Throughput Image Processing Software (HiTIPS) to expand the range and customization of existing HTI analysis capabilities. HiTIPS incorporates advanced image processing and machine learning algorithms for automated cell and nuclei segmentation, spot signal detection, nucleus tracking, nucleus registration, spot tracking, and quantification of spot signal intensity. Furthermore, HiTIPS features a graphical user interface that is open to integration of new analysis modules for existing analysis pipelines and to adding new analysis modules. To demonstrate the utility of HiTIPS, we present three examples of image analysis workflows for high-throughput DNA FISH, immunofluorescence (IF), and live-cell imaging of transcription in single cells. Altogether, we demonstrate that HiTIPS is a user-friendly, flexible, and open-source HTI software platform for a variety of cell biology applications.

High-Throughput Imaging (HTI) fully automates the acquisition and analysis of large fluorescence microscopy imaging datasets. HTI was originally developed to provide phenotypic readouts for large high-throughput chemical screens to identify compounds with desirable therapeutic activities<sup>1,2</sup>. Since then, this technology has also been widely adopted to work in conjunction with functional genomics screens to identify molecular pathways involved in a variety of cellular functions. Furthermore, HTI has been extensively implemented in more traditional cell biology applications, where the automation of image acquisition and analysis has been used to systematically quantify at the single-cell level phenotypes that are heterogeneous, rare, or dynamic in cellular populations<sup>3</sup>.

The study of nuclear architecture and gene expression has particularly benefited from HTI. DNA Fluorescence In Situ Hybridization (FISH)-based HTI imaging has been used to study the spatial organization of genes and chromosomes within the nucleus, providing insights into the mechanisms of gene regulation and nuclear architecture. For example, FISH-based HTI has been used to study the three-dimensional organization of the genome<sup>3-7</sup>. In addition, immunofluorescence (IF)-based HTI assays have helped probe nuclear architecture using fluorescently labeled endogenous architectural markers in combination with functional genomics screens<sup>8-13</sup>. Finally, HTI has also been used to explore the dynamics of transcription initiation and RNA splicing in live cells and at the single-cell level<sup>14,15</sup>.

HTI has been enabled by the development of automated microscopy platforms and image analysis software to rapidly acquire and process large amounts of fluorescence microscopy data. These tools allow the extraction of quantitative information at the single-cell level of many cellular features in individual cells<sup>16</sup>. Traditionally, software for HTI analysis has been structured around three major components: (1) individual analysis modules to perform basic HTI analysis steps (e.g., nuclear segmentation, spot detection, cell tracking, fluorescence intensity measurements), (2) a graphical user interface (GUI) for end-users without programming skills to set

<sup>1</sup>High-Throughput Imaging Facility, National Cancer Institute, National Institute of Health, Bethesda, MD 20892, USA. <sup>2</sup>Cell Biology of Genomes, National Cancer Institute, National Institute of Health, Bethesda, MD 20892, USA. <sup>3</sup>System Biology of Gene Expression, National Cancer Institute, National Institute of Health, Bethesda, MD 20892, USA. <sup>4</sup>Department of Biochemistry and Molecular and Cellular Biology, Georgetown University Medical School, Washington, DC 20057, USA. <sup>5</sup>These authors contributed equally: Faisal Almansour, Krishnendu Guin and Varun Sood. ✉email: gianluca.pegoraro@nih.gov

the parameters for the analysis modules in an interactive fashion, and (3) a mechanism to chain the analysis modules into end-to-end analysis pipelines that can be run in batch mode.

Previous open-source software tools, such as FISH-quant v2<sup>17</sup>, CellProfiler<sup>18,19</sup>, and others, have been introduced to tackle the wide demand for automated image analysis to study gene expression in fixed cells. However, there is still a need to develop open-source software that provides a graphical user interface (GUI) for users with no programming experience, that can adopt additional advanced spot finding methods, often essential to analyze images generated by DNA and RNA FISH HTI assays, and that can provide end-to-end analysis capabilities, such as detection, registration, and tracking of transcription sites in the nucleus to study the dynamics of gene expression in living cells<sup>14,15</sup>.

To address these needs, we developed an open-source HTI analysis software tool named High-Throughput Image Processing Software (HiTIPS). HiTIPS can be used to analyze a wide range of HTI imaging assays for the study of gene expression and nuclear biology, both in fixed and live cells. HiTIPS is built in Python, and it can be installed on multiple operating systems as a single module using common Python installers and environment management tools. In addition, we also provide a containerized version of HiTIPS to reduce the need for strict operating system configurations and the possibility of Python library installation issues due to changing versions of HiTIPS Python dependencies. To adhere to open science standards, and to facilitate HiTIPS adoption by the bioimaging research community, the HiTIPS code base is available as a Github repo. Furthermore, we provide extensive online software documentation regarding both installation and usage instructions, as well as detailed documentation about HiTIPS algorithms and its architecture. Importantly, HiTIPS provides a GUI for interactive and user-friendly visualization of images, and for the optimization of HTI analysis parameter settings without the need for coding. The GUI provides access to a variety of image analysis modules for HTI, which incorporate both traditional image processing algorithms, and advanced machine learning algorithms for nucleus segmentation and fluorescence signal spot detection. HiTIPS is built using a flexible architecture, which allows the incorporation of novel algorithms, and the addition of new analysis modules for additional HTI analysis tasks, making HiTIPS extensible and amenable to a wide variety of HTI assays.

As compared to other open-source software for image analysis, HiTIPS uniquely provides a series of novel advanced methods accessible through a GUI for tracking and registration of nuclei of live cells, and for tracking of spot like features, like fluorescently labeled mRNA molecules at transcription sites, in timelapse experiments. This last set of capabilities makes HiTIPS ideally suited for the high-throughput study of the dynamics of fluorescently labeled chromatin loci, mRNA molecules, and nuclear bodies to study the dynamics of 3D genome architecture, transcriptional bursting, nascent mRNA splicing, and of nucleus architecture.

## Results

### Image loading and visualization

HiTIPS is designed for easy setup and execution of HTI image analysis pipelines. Users can first use HiTIPS by optimizing analysis parameters in an interactive fashion on a subset of representative images, enabled by HiTIPS' ability to provide visual feedback of the results of the image analysis overlaid on the original images. Once this optimization process is completed, users can then run the analysis in batch mode on the whole image dataset. Both the interactive analysis module setup and launching the batch analysis pipeline steps in HiTIPS do not require programming, thanks to a GUI that is used for data loading, for image and results visualization, and for the choice of the image analysis modules parameters (Fig. 1A).

HiTIPS allows users to select HTI imaging datasets and to load selected data on demand, thus eliminating the need to retain the entire dataset in memory (Fig. 1A). This enables swift, efficient access to extensive image datasets, while minimizing memory requirements for processing. As an example, a 4-channel image from an HTI dataset can be typically loaded in less than 1.2 s on different hardware platforms (Supplementary Note 1). In addition, HiTIPS uses either a generic Bio-Formats reader<sup>20</sup>, which allows the loading and conversion of more than 120 different imaging formats, or it uses image acquisition metadata (well position, field of view (FOV), channel, etc.) automatically generated by the microscope and saved in separated XML files. While this second mechanism is currently only implemented for the CellVoyager format and for imaging datasets generated by Micro-Manager, a popular open-source microscope controlling and image acquisition software<sup>21</sup>, the open-source and modular nature of HiTIPS allows the future extension of metadata reading from files to other instruments and formats, potentially including the recently developed OME-ZARR format<sup>22</sup>. Thanks to the use of image acquisition metadata by HiTIPS, users can rapidly select specific wells, FOVs, and/or channels to quickly load single merged FOVs in the viewer for visual inspection of the images, and for optimization of the image analysis parameters (Fig. 1A).

Once the images are loaded, users can perform a series of routine changes to their visualization, including toggling specific channels on or off, showing a z-projected version of the image if the FOV is present as a 3D z-stack, and independently adjusting minimum and maximum intensity levels for each of the channels (Fig. 1B). Visual inspection of random wells and FOVs in the dataset is often an essential quality control step before setting up an HTI image analysis pipeline, and it is greatly facilitated by rapid loading and rendering of the images by HiTIPS. Furthermore, the image visualization interface is not limited to the original images, but also includes the overlaid presentation of object masks and borders generated by different image analysis modules that can also be selected and whose parameters can be modified using another window in the GUI (Fig. 1C). This is an essential feature that enables rapid cycles of parameter optimization during the interactive image analysis setup phase. Finally, after configuring the analysis parameters in interactive mode, HiTIPS allows users to choose the number of parallel processing threads for batch analysis depending on the technical specification of the hardware on which the application is running, either locally, or on an HPC cluster (See Methods and Supplementary Note 1 for details on hardware configurations).

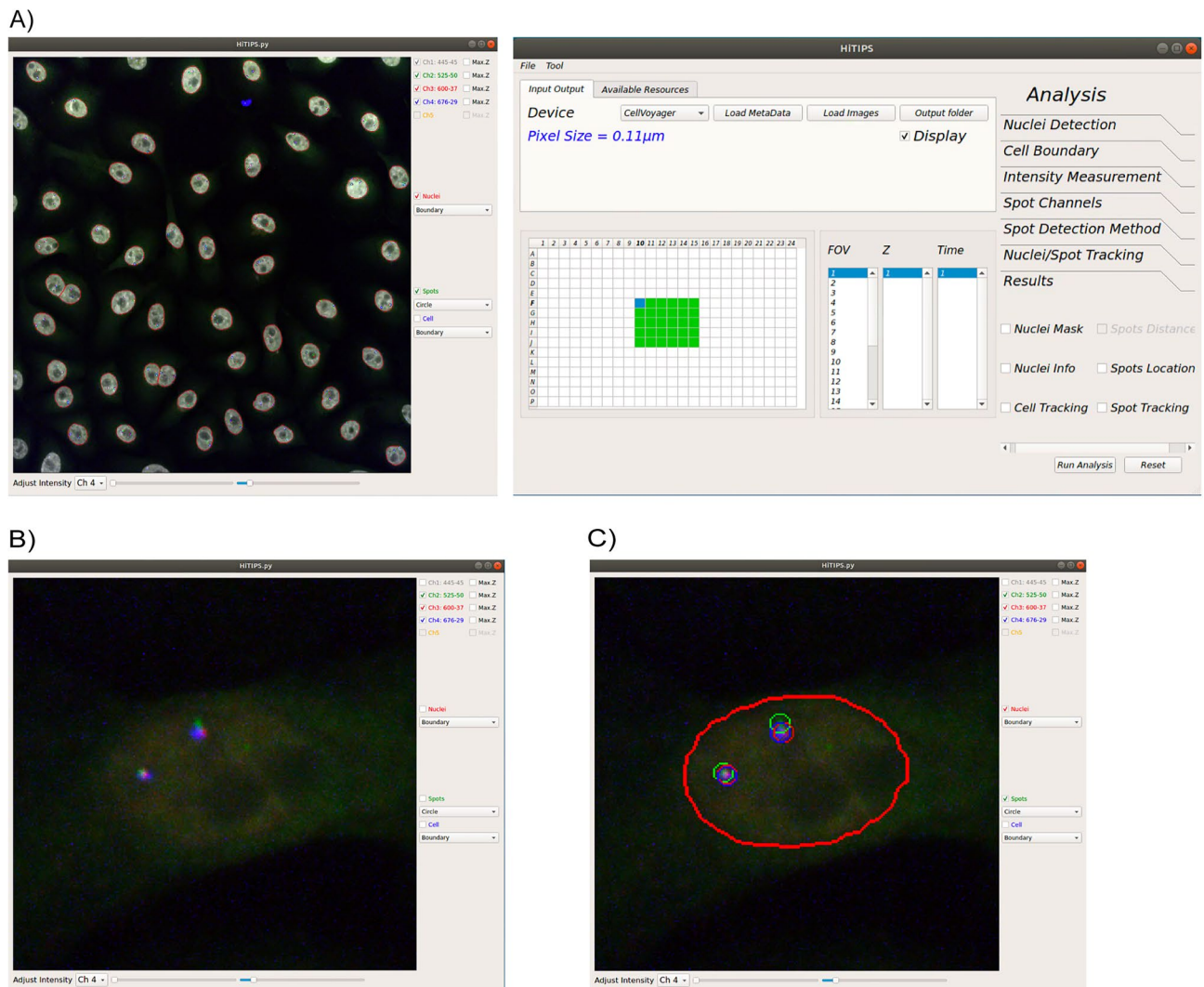


**Figure 1.** Examples of the HiTIPS GUI. (A) Representative screenshot of the HiTIPS GUI for HTI dataset selection and on-demand image loading, with metadata loading and integration in various formats, including CellVoyager and Micro-Manager. (B) Representative screenshot of the image visualization controls in the HiTIPS GUI, including, fluorescence channel toggling and z-projected views for 3D z-stacks, and fluorescence intensity visualization adjustment. (C) Representative screenshot of the overlaid display in the HiTIPS GUI of nuclei masks borders (red) and spot detection in 2 different channels (red and green circles) output from image HiTIPS analysis modules.

### HTI image analysis workflow

While HiTIPS was built to analyze a variety of HTI assays, and it can further be extended or customized by a developer to accommodate additional specific analysis needs, we used genome architecture and gene expression assays in both fixed and live cells as model systems for our initial efforts in the development of HiTIPS. For this reason, the HiTIPS analysis workflow currently includes sequential use of image and metadata loading (Fig. 2, i), nuclei segmentation (Fig. 2, ii), fluorescent spot finding (Fig. 2, iii), nuclei tracking (Fig. 2, iv), nuclei and spot patch generation (Fig. 2, v), nuclei and spot patch registration (Fig. 2, vi), spot assignment to a track (Fig. 2, vii), measurement of fluorescence intensity (Fig. 2, viii), and 2-state Hidden Markov Model (HMM) fitting to segment fluorescence intensity traces (Fig. 2, ix). While the modular structure of HiTIPS allows to adopt already existing state-of-the-art algorithms and models, such as for nuclear segmentation, tracking, and integrated spot fluorescence calculations, several of the algorithms used in these pipelines, including spot finding, nucleus registration, and spot tracking are novel and optimized for live cell imaging of gene expression (See Methods and Supplementary Note 2). HiTIPS also allows the selection of the workflow steps only up to the spot finding module (Fig. 2, i–ii), or up to the nucleus tracking module for live-cell HTI assays that do not require spot level measurements (Fig. 2, i, ii, and iv). This selection can be performed by toggling specific modules on or off in the GUI (Fig. 1A) during the interactive setup phase of image analysis workflow. Additional usage instructions on how to use HiTIPS, and detailed documentation for all the analysis modules and algorithms implemented, can be found at the online documentation page for HiTIPS, and in Supplementary Note 2.

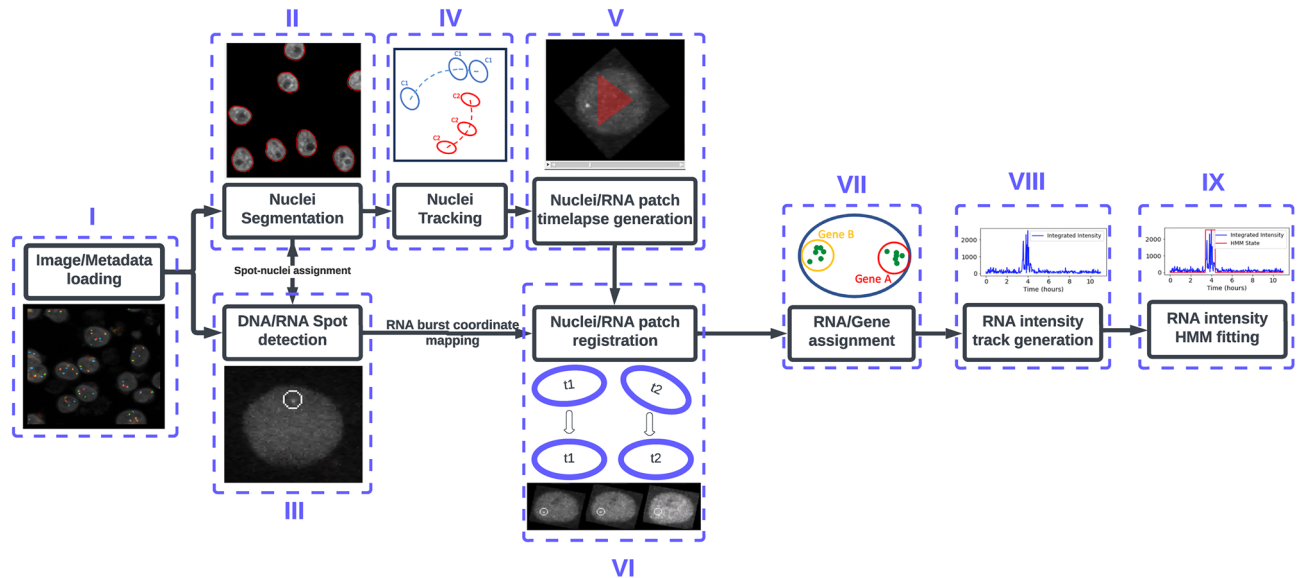


**Figure 2.** Schematic representation of the full HiTIPS image analysis workflow. (i) Image and metadata loading, leading to (ii) Nuclear segmentation and (iii) Spot finding, (iv) Nucleus tracking (v) Single nucleus timelapse generation, and (vi) Frame to Frame nuclei registration processes. (vii) Spot assignments to specific tracks are determined before (viii) Measurement of track fluorescence intensities, culminating in (ix) Segmentation of gene ON and OFF states by fitting a 2-state Hidden Markov Model (HMM) to the fluorescence intensity tracks.

To show the utility of HiTIPS across a broad spectrum of data types and applications related to the biology of the cell nucleus, we applied it to three distinct HTI assays: (1) measurement of 3D physical distances between two genomic loci visualized with DNA FISH probes, (2) estimation of spatial clustering in the nucleus of centromeres labeled by IF with an antibody to the centromeric protein CENPC, and (3) a set of high-throughput measurements of transcriptional activity in live cells of the endogenous *KPNB1* or *ERRF1* genes labeled with the fluorescent MS2/MCP-GFP system.

### HiTIPS measures spatial distances between genomic loci in high-throughput fashion

Mammalian genomes are spatially organized in the cell nucleus at several different hierarchical levels, and 3D genome organization is tightly correlated with many nuclear functions such as transcription, replication, and DNA damage repair<sup>23</sup>. A prominent feature of genome organization are Topologically Associating Domains (TADs), which represent genomic regions which exhibit an enhanced propensity for mutual interaction, across relatively large genomic distances (200 kb–1 Mb)<sup>23,24</sup>. At the molecular level, one of the key factors for TAD establishment and maintenance is the cohesin complex, as demonstrated by the observation that acute depletion of the RAD21 cohesin subunit leads to loss of these domains as measured by biochemical chromatin conformation capture techniques<sup>25</sup>, and to an increase in physical distances between adjacent TADs as measured by DNA FISH imaging<sup>26</sup>.

We wanted to test HiTIPS in a high-throughput DNA FISH assay to see whether we could measure changes in the physical distances of the boundaries of the TAD containing the human *EGFR* gene on Chr 7 upon acute depletion of RAD21 (Fig. 3A). To this end, we performed high-throughput DNA FISH imaging experiments in HCT116-RAD21-AID cells, where RAD21 can be rapidly degraded by the cellular ubiquitin/proteasome machinery upon binding of the AID degenon domain to Auxin as previously described<sup>27</sup> (Fig. 3A). We used automated confocal imaging to acquire z-stack images of HCT116-RAD21-AID cells treated for 3 h with Auxin or mock treated cells in 3 channels (DAPI, EGFR TAD 5' boundary/Probe A, EGFR 3' boundary/Probe B, Fig. 3B). 3D image stacks were analyzed with HiTIPS in batch by segmenting nuclei using the DAPI image, by finding the position of FISH spots in 3D, and by calculating minimum distances between FISH spot centers in the two different channels on a per allele basis (Fig. 2, i–iii). After plotting the distributions of minimum distances between the genomic loci at the base of the loop domain in 1874 cells in either Auxin-treated or mock-treated control cells, we observed that RAD21 degradation upon Auxin treatment led to a statistically significant increase in the distance between TAD boundaries (Fig. 3C,  $p < 2e-16$ , Wilcoxon Test). These results show that HiTIPS can be used for the automated analysis of 3D distances measured from DNA FISH images.

### Clustering analysis of centromeres in the nucleus

Centromeres are specialized genomic regions that assemble the kinetochore, a large protein complex consisting of several components, including the evolutionarily conserved CENPC protein<sup>28</sup>. Kinetochores physically connect chromosomes to microtubules and ensure high-fidelity genome segregation during cell division<sup>29</sup>. Centromere positions within the 3D space of the cell nucleus vary across species<sup>30</sup>. Recently, it was shown that loss of the

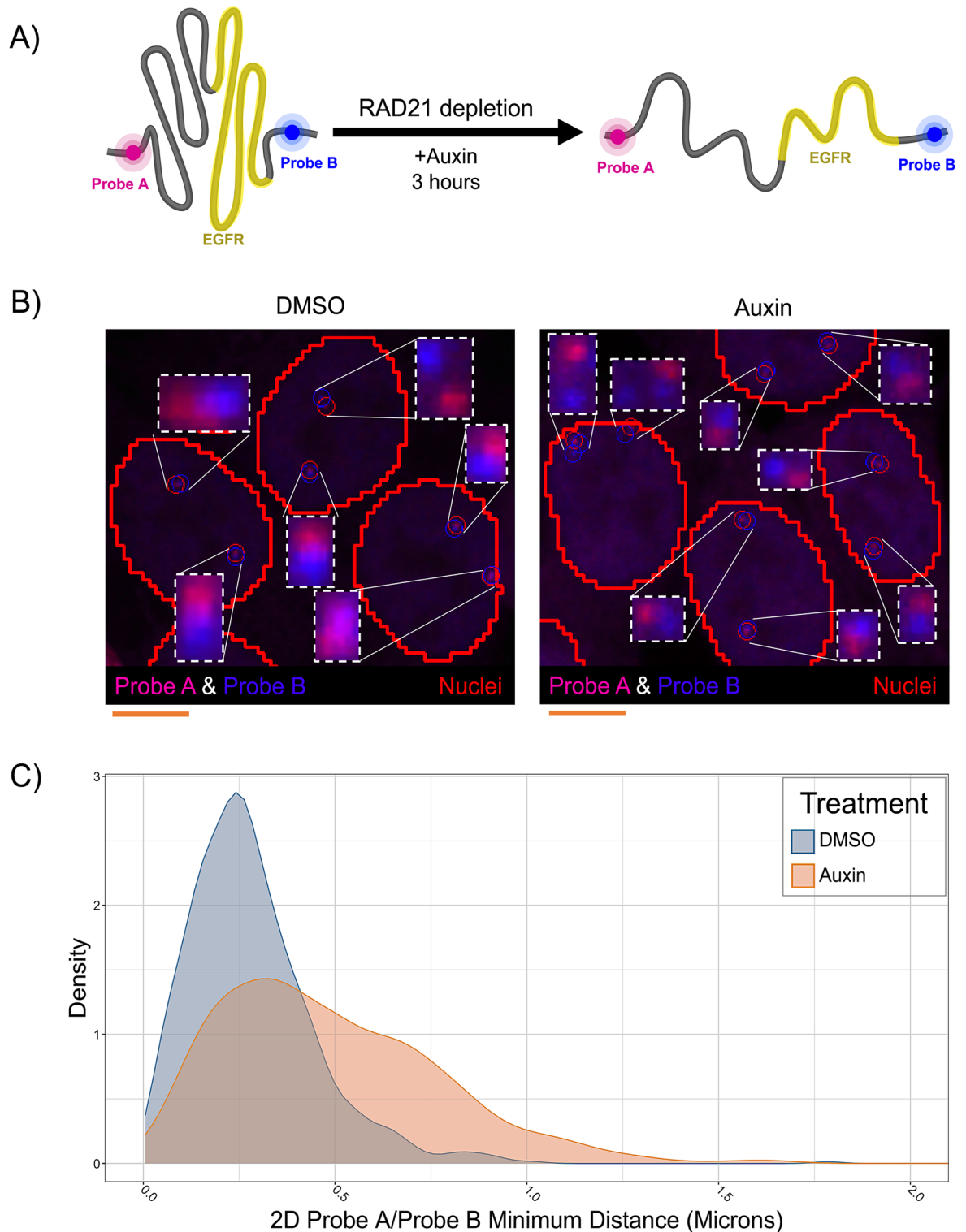


**Figure 3.** HiTIPS measures distances between genomic loci labeled with High-Throughput DNA FISH probes. **(A)** Schematic representation of the experiment to measure spatial distances of two genomic loci located at the base of a TAD encompassing the *EGFR* gene on Chr 7 and detected by FISH probes in different channels (Probe A and Probe B). Treatment with Auxin in HCT116-RAD21-AID cells leads to rapid proteolytic degradation of the RAD21-AID fusion protein via the ubiquitin/proteasome pathway. **(B)** Representative 3D maximally projected images of HCT116-RAD21-AID cells stained with DNA FISH probes A and B targeted to the 5' and 3' boundaries of the *EGFR* TAD, respectively, and of the results of the HiTIPS spot finding algorithm results overlaid as red and blue circles, respectively. Scale bar: 5 microns. **(C)** Density plots of minimum spatial distances between the A and B DNA FISH probes in 1874 cells treated with Auxin or DMSO.

condensin II complex subunit NCAPH2 leads to centromere clustering in human cancer cells using biochemical techniques and traditional low-throughput fluorescence microscopy<sup>31</sup>.

We tested whether we could use HiTIPS to measure spatial clustering of centromeres at the single-nucleus level (Fig. 4). To this end, we reverse-transfected HCT116-Cas9 cells with siRNA oligos against the *NCAPH2* gene, or a scrambled negative siRNA control in 384-well plates. Cells were fixed and stained with DAPI for nuclei segmentation and with a CENPC-specific antibody to visualize centromeres. Stained cells were then imaged in 3D (Fig. 4A), and maximally projected images were analyzed using HiTIPS for nuclear segmentation and spot finding/localization (Fig. 2, i–iii). HiTIPS was capable to precisely detect and localize CENPC spots in cell nuclei, even in regions of high density of CENPC spots (Fig. 4A). More importantly, the single CENPC spot position datasets and the nuclei ROIs could be used in a separate analysis to calculate a centromeric clustering score in single cells. We defined this score as the percentage of the measured curve for Ripley's K function<sup>32</sup> that is above the curve for the random Poisson distribution (See Materials and Methods for details). This clustering analysis showed that, in line with visual inspection, cells transfected with siNCAPH2 had higher clustering scores (Fig. 4B) and fewer distinguishable centromeres (Fig. 4C) than cells transfected with the control scrambled siRNA. These results show the utility of HiTIPS in the analysis of IF-based HTI assays at the single-cell level, and they confirm previous traditional fluorescence microscopy-based results<sup>31</sup>, while expanding the phenotypic analysis from a few cells to thousands of cells.

### Semi-automated measurement of transcription dynamics at the single-allele level in live cells

Random or targeted intronic integration of endogenous genes with arrays of MS2 hairpins in cells stably expressing a fluorescently tagged fusion of the MS2 capsid protein (MCP) has been instrumental in demonstrating that in mammalian cells transcription happens in bursts of activity followed by periods of inactivity<sup>33</sup>, and that splicing of long introns is recursive<sup>15</sup>. HTI acquisition and analysis have been used to measure the dynamics of these events in large numbers of single live cells<sup>14,15</sup>.

We aimed to test whether the novel algorithms we developed in HiTIPS for spot finding, nucleus tracking, nucleus registration, and spot tracking could reproduce the results of our previous image analysis pipeline<sup>15</sup> and to show that HiTIPS can be applied to precisely quantify transcriptional dynamics in live cells at the single-cell level (Fig. 5). To this end, we ran the full HiTIPS analysis pipeline on HTI datasets from two clonal human

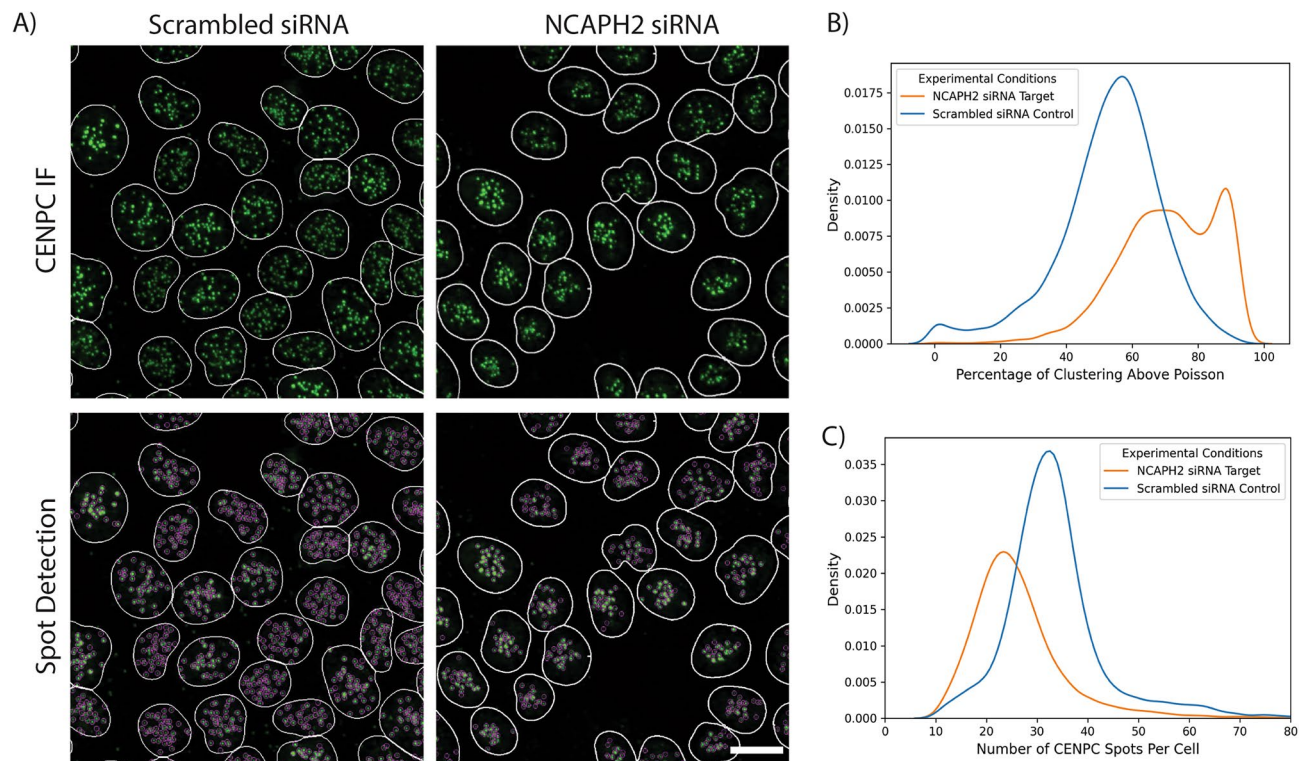


**Figure 4.** HiTIPS analysis of centromeric clustering. (A) 3D maximally projected images of HCT116-Cas9 cells reverse transfected in 384-well plates for 72 h with either a scrambled non-targeting siRNA (siScramble), or with a siRNA against the condensin II subunit NCAPH2 (siNCAPH2). Transfected cells were stained by IF with DAPI and a CENPC antibody, and imaged using a high-throughput confocal spinning disk microscope. The border of the segmented nuclei masks is overlaid on the image and colored in white. CENPC spots detected by HiTIPS are overlaid as magenta circles in the lower images. Scale bar: 10 microns. (B) Density plot of cell-level CENPC spots clustering scores for siScramble and siNCAPH2 as calculated by HiTIPS. Higher values of the clustering score indicate more clustering of CENPC spots in the nucleus. (C) Density plot of the number of CENPC spots per cell for siScramble and siNCAPH2 as calculated by HiTIPS.

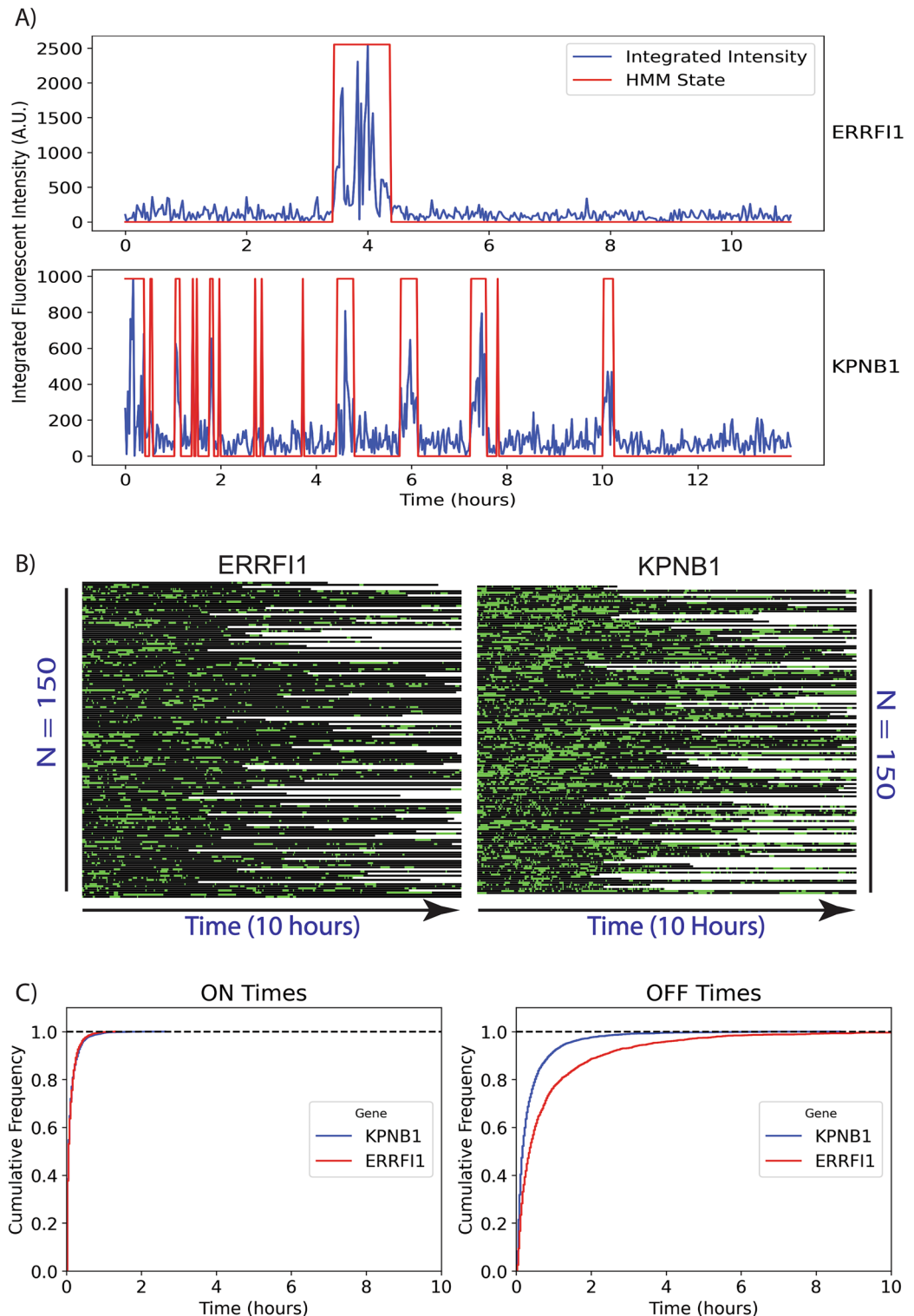


**Figure 5.** HiTIPS quantifies gene expression dynamics in live cells. **(A)** Normalized and integrated fluorescence intensity plot at the site of MS2/MCP-GFP spots detected in live cells over 10 h for both MS2-tagged *ERRFI1* and *KPNB1* genes. The HMM 2-state segmentation of intensity traces into “ON” and “OFF” times is indicated in red. **(B)** Kymograph of 2-state HMM-segmented fluorescence intensity traces for a sub-sample of fluorescence intensity traces ( $n = 150$  for *ERRFI1*-MS2/MCP-GFP and  $n = 150$  for *KPNB1*-MS2/MCPGFP) over 10 h. Green represents “ON” times (active transcription), black represents “OFF” times (no transcription) in the kymograph. **(C)** Empirical cumulative distribution function plots of ON and OFF time durations for both cell lines across multiple cells and transcription sites ( $n = 260$  for *KPNB1*-24xMS2/MCP-GFP and  $n = 260$  cells for both *ERRFI1*-24xMS2/MCPGFP).

bronchial epithelial (HBEC) cell lines, in which the *ERRF1* and *KPNB1* genes have been endogenously tagged with 24xMS2 loops, enabling visualization of their nascent transcription with MCP-GFP<sup>15</sup>. MS2/MCP-GFP labeled transcription sites in these nuclei were detected (Fig. 2, iii), registered (Fig. 2, vi), grouped into tracks (Fig. 2, vii), and the integrated fluorescence intensity was measured at the site of transcription (Fig. 2, viii).

This automated analysis resulted in the generation of 1232 fluorescence intensity traces (690 for *ERRF1*-24xMS2/MCP-GFP and 542 for *KPNB1*-24xMS2/MCP-GFP). We further conducted a visual quality control step on the segmented transcription site traces to obtain a total of 595 traces (277 for *ERRF1*-24xMS2/MCP-GFP and 318 for *KPNB1*-24xMS2/MCP-GFP). In agreement with previous work<sup>15</sup>, visualization of a subset of fluorescence intensity traces for single alleles of *ERRF1* and *KPNB1* revealed that *KPNB1* bursts more frequently than *ERRF1*, due to shorter periods of inactivity (OFF times) (Fig. 5A). Extending this analysis to a larger sub-sample of fluorescent intensity traces for each cell line (Fig. 5B,  $n = 150$  for *ERRF1*-24xMS2/MCP-GFP, and  $n = 150$  for *KPNB1*-24xMS2/MCP-GFP) confirmed that the observed difference in transcriptional dynamics of *KPNB1* and *ERRF1* extends to the cellular population. Further evidence supporting this observation comes from analysis of cumulative distributions of ON and OFF times across an even larger sub-sample of all the intensity traces (Fig. 5C,  $n = 260$  for *ERRF1*-24xMS2/MCP-GFP, and  $n = 260$  for *KPNB1*-24xMS2/MCP-GFP). We observed that *ERRF1* has on average significantly longer OFF times compared to *KPNB1*, while the distribution of ON times is not substantially different between the two genes. These results obtained with the HiTIPS pipeline are consistent with previous observations<sup>15</sup>: differences in transcriptional dynamics between different genes in human cells correlate with variation in bursting frequency (OFF times), while ON times distributions for different genes remain largely invariant. Overall, these results indicate that HiTIPS can reliably measure the dynamics of transcription in an automated manner and for hundreds to thousands of live cells in long time-lapse experiments.

## Discussion

We developed HiTIPS as an open-source and automated image analysis software for large HTI datasets, equipped with advanced methods for FISH and/or IF spot detection, and with novel custom algorithms for spot detection, nucleus registration, and spot registration/tracking in time-lapse datasets of live cell gene expression imaging.

Individual researchers and imaging core facilities frequently struggle with identifying HTI software that combines ease-of-use for researchers with no programming experience with the flexibility to incorporate new analysis modules and algorithms for image bioinformatics developers. In developing HiTIPS, we strived to find a balance between these two needs. We believe that HiTIPS achieves this by taking advantage of a flexible GUI for both HTI datasets visualization and analysis parameter optimization (Fig. 1). This functionality not only allows for the optimization of analysis methods and parameter adjustments but also supports the exploration of multi-well plate datasets and multi-channel visualizations. In addition, HiTIPS is written using Python, one of the most commonly used open-source programming languages in the biological image analysis and machine learning fields. The modular construction of HiTIPS allows the adoption and integration of existing state of the art image analysis algorithms (such as the Enhanced Gaussian Filter and Laplacian for spot finding) and deep learning models (such as Cellpose for nucleus segmentation). At the same time, by using a modular software architecture that allows the incorporation of not only new algorithms for existing analysis modules (e.g. nuclear segmentation, spot finding, etc.), but also of completely new HTI analysis modules.

As proof of principle, we have used HiTIPS for the analysis of HTI assays designed to address biological questions related to nuclear architecture and gene expression, in both fixed and live cells. We show that HiTIPS performs robustly for nuclear segmentation, nucleus tracking, spot detection, and spot tracking. In addition, HiTIPS can be used to measure fluorescence intensity, morphology, and kinetics measurements for nuclear compartments or markers at the single-cell level (Fig. 2). We used these HTI measurements to address a variety of questions related to 3D genome architecture (Fig. 3), centromere biology (Fig. 4), and transcriptional dynamics (Fig. 5). The results of these studies highlight HiTIPS' ability to analyze data from HTI assays incorporating various fluorescent sample preparation techniques (FISH, IF, recombinant fluorescent proteins) and in both fixed and live cells.

We consider HiTIPS a user-friendly addition to the suite of open-source software platforms available for HTI analysis. As compared to some these, HiTIPS has both advantages and limitations. ImageJ<sup>34</sup> has long been one of the most used and flexible open-source software for bioimage analysis and it has a rich plugin ecosystem to extend its capabilities in image visualization and analysis. As a generalist analysis tool, ImageJ can clearly handle a larger number of image analysis tasks but is not geared toward automated high-throughput image analysis using automated pipelines, which is the main design focus of HiTIPS. Cellprofiler<sup>18,19</sup> is another widely adopted and flexible open-source image analysis software with extensive capabilities for HTI analysis, which provides more analysis modules options, has a more flexible framework to build the image analysis pipelines, and covers a wider range of HTI analysis use cases as compared to HiTIPS. In addition, other generalist open-source image analysis software tools are designed to excel at image visualization of complex multidimensional datasets, such as Napari<sup>35</sup> and MoBIE<sup>36</sup>, or for cell segmentation and morphology assessment, such as GIANI<sup>37</sup> and Tonga<sup>38</sup>. When compared with these latter software tools, HiTIPS uniquely provides a GUI that is specifically optimized for the selection and loading of multichannel images from a multi-well plate format common in HTI experiments. In addition, HiTIPS image analysis modules provide custom spot finding algorithms that are specifically designed for sensitive detection of FISH spots in fixed cells and fluorescent mRNA spots in live cells. Furthermore, HiTIPS also uniquely provides analysis modules for high-throughput nucleus and spot registration, spot fluorescence intensity calculations, and HMM fluorescent traces segmentation, which are necessary elements for the automated analysis transcription, splicing, and chromatin dynamics at the single allele level in time lapse experiments. All these modules are not available as a single pipeline in the above-mentioned software platforms. Finally, KNIME<sup>39</sup> and KNIP<sup>40</sup> have also been used by our groups<sup>14,15,41,42</sup> and others in combination with custom Python



scripts that were called inside KNIME pipelines for a range of advanced HTI image analysis pipelines to study gene expression, splicing, and nuclear architecture. While KNIME and KNIP provide an excellent set of tools for HTI image visualization and high-throughput analysis, HiTIPS has the advantage of being written in pure Python. Consequently, HiTIPS relies on a simplified software stack when compared to KNIME and KNIP. The reduced number of software dependencies make it easier to develop, document, and maintain HiTIPS. Furthermore, fewer software dependencies facilitate sharing HiTIPS with the open-source bioimage analysis community.

Like HiTIPS, FISH-quant v2<sup>17</sup>, dypFISH<sup>43</sup>, RS-FISH<sup>44</sup> are open-source software applications specialized in the analysis of FISH images, and have dedicated advanced algorithms and analysis modules for spot detection. dypFISH and RS-FISH do not have nucleus segmentation capabilities, while FISH-quant v2 is similarly aligned with HiTIPS in terms of design choices: it is an image analysis pipeline that includes a web GUI for visualization based on ImJoy<sup>45</sup>, it can perform nucleus segmentation using deep learning algorithms such as Cellpose, it provides advanced spot finding algorithms for smFISH images, and it calculates spot localization features that can be used to classify cells based on specific mRNA localization patterns, the latter being a feature that HiTIPS does not provide out of the box. On the other hand, HiTIPS can run a full image analysis pipeline for live cell time-lapse experiments, whereas FISH-quant v2 is limited to fixed FISH and IF experiments. In summary, each open-source software image analysis software has its own strengths and limitations based on the range of applications (e.g. generalist vs. specialized, single image vs. high-throughput, etc.), and several existing applications for bioimage analysis excel in their own application space. In this context (See Supplementary Note 3), HiTIPS is a user friendly, GUI-based HTI analysis platform that can be used to rapidly select, load, and visualize multichannel images from multi-well plate layouts, to quickly and interactively optimize image analysis parameters, and to run batch image analysis pipelines with advanced spot finding, nucleus tracking, nucleus registration, and spot tracking for both FISH and live cell experiments.

In the future, we expect that additional algorithms for FISH spot detection, such as the one present in FISH-quant v2<sup>17</sup>, dypFISH<sup>43</sup>, or RS-FISH<sup>44</sup>, and for nucleus segmentation and tracking, will be added to HiTIPS. Furthermore, as a natural progression for HiTIPS, we also foresee the addition of modules to segment the cell body and cell membranes, to extend the range of biological questions to other cellular compartments beside the nucleus. Similarly, we envision the potential addition of analysis modules in HiTIPS to measure fluorescence texture properties, additional morphological properties, and relational/cell neighborhood properties. Given the open-source and modular software architecture of HiTIPS, we hope that the biological image analysis community will contribute to the development of these new HiTIPS features.

## Methods

### siRNA oligos transfection and immunofluorescence

HCT116-Cas9 cells<sup>46</sup> were grown in RPMI-1640 medium (ATCC, Cat. No. 30-2001) supplemented with 10% fetal bovine serum (FBS, Gibco, Cat. No. 10-082-147) and maintained at 37°C in 5% CO<sub>2</sub>. siRNA oligos reverse transfection and immunofluorescence staining were performed in 384-well glass bottom plates (CellVis, Cat. No. P384-1.5H-N). The siRNAs used were siNCAPH2 (Thermo Fisher Scientific, Cat. No. 4392420, Assay ID s26585), and siScrambled (Thermo Fisher Scientific, Cat. No. 4390847). For reverse transfection, 150 nl of 5 M siRNA and 50 nl of Lipofectamine RNAiMAX reagent (Invitrogen, Cat. No. 13778075) were individually diluted in 20 µl of serum-free OptiMEM medium (Thermo Fisher Scientific, Cat. No. 31985070) and sequentially added to each well. The siRNA and RNAiMAX mix was incubated for 30 min at RT. Cells were trypsinized, and a cell suspension (2000 cells in a volume of 20 µl) was prepared in OptiMEM supplemented with 20% FBS. 20 µl of the cell suspension was added to each well containing the RNAiMAX/siRNA oligo complexes. Transfected cells were grown for 72 h in a cell incubator at 37°C and then fixed with 2% paraformaldehyde (PFA, Electron Microscopy Sciences, Cat. No. 15710) in PBS. Fixed cells were washed three times with PBS. Cells were then permeabilized using a 0.5% Triton X-100 (Milipore Sigma, Cat. No. 9036-19-5) solution in PBS for 15 min at RT, washed three times with 50 µl of PBS, and blocked in a 5% BSA (Milipore Sigma, Cat. No. 9048-46-8) solution in PBS for 15 min at RT. Immunofluorescence staining against the centromere protein CENPC was performed using a primary CENPC antibody (MBL Bio Science, Cat. No. PD030, raised in Guinea pig) at 1:1000 dilution for 1 h at RT, and a Goat Anti-Guinea pig IgG H&L secondary antibody (AlexaFluor 488, Abcam, Cat. No. Ab150185) at 1:500 dilution for 1 h at RT. For nuclear staining, 40 µl of a 5 mg/ml solution of 4',6-diamidino-2-phenylindole (DAPI, Thermo Fisher Scientific, Cat. No. 62248) in PBS were added to each well.

### High-throughput DNA FISH

HCT116 RAD21-mAID-mClover (HCT116-RAD21-AID) cells<sup>27</sup> were grown at 37 °C in 5% CO<sub>2</sub> in McCoy's 5A medium supplemented with 10% FBS, 2 mM L-glutamine, 100 U/ml penicillin, and 100 µg/ml streptomycin. For FISH experiments, cells were plated at a density of 8000 cells per well in 384-well imaging plates (PhenoPlate 384-well, Revvity, Cat. No. 6057500) and grown overnight. The following day, the medium was replaced with either supplemented medium containing 170 mM Auxin (Sigma-Aldrich, Cat. No. I3750) to induce the degradation of RAD21, or with medium with an equivalent amount of DMSO alone as vehicle control. The cells were then incubated with or without Auxin for 3 h and fixed in 4% PFA (Electron Microscopy Sciences, Cat. No. 15710) in PBS for 10 min. After fixation, the plates were rinsed three times in PBS and stored in PBS at 4 °C.

We conducted high-throughput fluorescence in situ hybridization (hiFISH) as previously described<sup>4,47</sup>. BAC FISH probes were selected to hybridize to the boundary regions of the topologically associated domain (TAD) on chromosome 7 containing the *EGFR* gene. Fluorescently labeled BAC probes were generated by nick translation at 14 °C for 1 h and 20 min. The reaction mixture included 40 ng/ml DNA, 0.05 M Tris-HCl pH 8.0, 5 mM MgCl<sub>2</sub>, 0.05 mg/ml BSA, 0.05 mM dNTPs (including fluorescently tagged dUTP), 1 mM β-mercaptoethanol, 0.5 U/ml *E. coli* DNA Polymerase, and 0.5 mg/ml DNase I. The reaction was stopped by adding 1 µl of EDTA per

50  $\mu$ l reaction volume, followed by a heat shock at 72 °C for 10 min. Probes were labeled either with DY549P1-dUTP (Dyomics, Cat. # 549P1-34) or with DY647P1-dUTP (Dyomics, Cat. # 647P1-34). The reaction was then stored at -20 °C overnight. Next, the two probes (0.5 mg per probe) were combined, precipitated with ethanol, and resuspended in 14  $\mu$ l of hybridization buffer (50% formamide pH 7.0, 10% dextran sulfate, and 1% Tween-20 in 2X SSC) per well. Cells were rinsed twice with PBS and subjected to permeabilization. Permeabilization was performed at room temperature for 20 min using 0.5% w/v saponin/0.5% v/v Triton X-100 in PBS. After rinsing the cells with PBS twice, cells were deproteinized for 15 min in 0.1 N HCl and neutralized for 5 min in 2X SSC at room temperature. Cells were equilibrated overnight in 50% formamide/2X SSC at 4 °C. The probe mix was warmed to 72 °C prior to the hybridization reaction. Next, 14  $\mu$ l/well of resuspended probe mix was added to the plate and denatured at 85 °C for 7 min, followed by immediate transfer to a 37 °C incubator for a 48-h hybridization period. Post-hybridization, plates were rinsed once at room temperature with 2X SSC, followed by three rinses with 1X SSC and 0.1X SSC, all warmed to 45 °C. Cells were stained with 3  $\mu$ g/ml DAPI for 15 min, then rinsed and mounted in PBS and subsequently imaged on a high-throughput confocal microscope.

### High-throughput live cell imaging of transcription

For the live cell transcription assay, human bronchial epithelial cell lines (HBEC3-KT) with a monoallelic insertion of an MS2 array in the intron of the model genes were used, as previously described<sup>15</sup>. To enable visualization of the nascent RNA, the viral MS2 capsid protein (MCP) fused to GFP and to an NLS (nuclear localization signal) tag was stably introduced into the cells using lentiviral expression vectors<sup>48</sup>. Cells were grown in Keratinocyte serum-free medium (Thermo Fisher Scientific, Cat. No. 17005042) supplemented with bovine pituitary extract (Thermo Fisher Scientific, Cat. No. 13028014) and human growth hormone (Thermo Fisher Scientific, Cat. No. 1045013). For imaging experiments, cells were cultured in 384 well plates (PhenoPlate 384-well, Revvity, Cat. No. 6057500) and imaged at 37 °C, 5% CO<sub>2</sub>, 80% humidity.

### High-throughput image acquisition

High-throughput imaging was performed using either a Yokogawa CV7000 or a CV8000 high-throughput spinning disk confocal microscopes.

For DNA FISH experiments, we used 405 nm (DAPI Channel), 561 nm (Probe A channel), or 640 nm (Probe B channel) excitation lasers. In addition, we used a 405/488/561/640 nm excitation dichroic mirror, a 60X water objective (NA 1.2), and 445/45 nm (DAPI Channel), 600/37 nm (Probe A channel), or 676/29 nm (Probe B channel) bandpass emission mirrors in front of a 16-bit sCMOS camera (2048  $\times$  2048 pixel, binning 1X1, pixel size: 0.108 microns). Z-stacks of 7 microns were acquired at 1 micron intervals and maximally projected on the fly. Images were acquired in 32 fields of view (FOV) per well.

For IF experiments, we used 405 nm (DAPI Channel) or 488 nm (CENPC channel) excitation lasers, a 405/488/561/640 nm excitation dichroic mirror, a 60X water objective (NA 1.2), 445/45 (DAPI Channel) or 525/50 nm (CENPC Channel) bandpass emission mirrors, and a 16-bit sCMOS camera (2048  $\times$  2048 pixel, binning 1X1, pixel size: 0.108 microns). Z-stacks of 14 microns were acquired at 1 micron intervals and maximally projected on the fly. Images were acquired in 22 FOV per well.

For live cell imaging experiments, we used a 488 nm excitation laser, a 405/488/561/640 nm excitation dichroic mirror, either a 40X air objective (NA 0.95) or a 40X water objective (NA 1.15), a 525/50 nm bandpass emission mirror, and a 16-bit sCMOS camera (2048  $\times$  2048 pixel, binning 2X2, pixel size: 0.325 microns). Z-stacks of 0.5 microns were acquired at 100 s intervals and maximally projected on the fly for 10 h.

In all cases, images were corrected on the fly with Yokogawa proprietary software to subtract the camera dark background, to compensate for illumination artifacts (vignetting), and for chromatic aberrations and camera alignment.

### HiTIPS implementation

HiTIPS uses the PyQt5 Python module, which offers a user-friendly GUI enabling interactive data analysis. Its architecture implements multiprocessing to optimize computational efficiency, a critical aspect when dealing with large-scale bioinformatics datasets. The parallel processing scheme in HiTIPS is designed to completely analyze (nuclei segmentation, spot detection etc.) each FOV in a separate thread. Depending on the available hardware, parallel processing in HiTIPS can reduce the analysis time by 5- to 8-fold, depending on the analysis workflow.

HiTIPS depends on several Python scientific computing libraries, including numerical computation and data manipulation (SciPy, Pandas), image processing (Pillow, Matplotlib, imageio, scikit-image, and OpenCV), dynamic cell tracking (btrack), machine learning-based image segmentation and classification (DeepCell<sup>49</sup> and Cellpose<sup>50</sup>), image input/output and format conversion (aicsimageio, nd2reader), and Hidden Markov Model fitting (hmmlearn). At least 8 GB of RAM are required to run HiTIPS, but having 32 GB of RAM may be required for larger FOVs and for 3D volumes. In addition, when using deep learning based nuclear segmentation or cell tracking models in HiTIPS (i.e., Cellpose and DeepCell), the availability of graphical processing units (GPUs) substantially improves the inference speed of these models. Additional details about the specifications for typical hardware configurations can be found in Supplementary Note 1, while details about the implementation of the pipeline in code can be found in Supplementary Note 4.

### Nucleus segmentation

Nucleus segmentation using images of nuclei stained with a fluorescent dye or a recombinant fluorescent nuclear protein is the key first step in the vast majority of HTI analysis pipelines. Given the high relevance of this step for HTI, a substantial amount of work in the field has been devoted to making nuclear segmentation algorithms fast, precise, and robust to fluctuations in cell confluency and to heterogeneity in nucleus morphology across

different cells<sup>51</sup>. For this reason, and to take advantage of previous advances made by other groups, we focused on integrating existing state-of-the-art nucleus segmentation algorithms into HiTIPS so that end users can easily access them and modify their parameters if needed. Accordingly, the HiTIPS GUI allows users to choose among a traditional CPU based method (Supplementary Note 2, Algorithm 1) for segmentation in the nucleus segmentation module, which we have developed to handle cases that do not necessarily require deep learning models, which require high-end graphical processing units (GPUs). In addition, HiTIPS also adopts two recent deep learning-based methods for nuclear segmentation, Cellpose<sup>50,52</sup> and DeepCell<sup>53</sup>. Deep learning-based nuclei segmentation models do not involve time consuming parameter optimization, and they generally provide excellent segmentation performance on a variety of different cell lines “out-of-the-box”. On the other hand, the speed performance of segmentation models really benefits from access to GPUs, which tend to be expensive and difficult to setup for end users. Traditional image processing algorithms for nucleus segmentation can be fast if properly optimized and can handle a variety of edge cases upon expert parameter optimization. The watershed-based segmentation method is the CPU-based approach integrated into HiTIPS. It starts with image padding and noise reduction via median filtering, followed by image binarization using Li’s iterative method<sup>54</sup>. The binary image is then processed using morphological operations and a Gaussian kernel to connect fragmented nuclei. The method labels connected components and it calculates the center of mass for each, creating a new mask image. A watershed transform<sup>55</sup> is applied using this mask and the distance-transformed image to separate adjacent nuclei effectively. Finally, a boundary image is created, resized to the original size, and any holes are filled to generate the final mask. By providing an easy selection of different nuclear segmentation methods via a GUI, HiTIPS allows users to choose and optimize the method that works best on their images and in the context of the available computational hardware infrastructure.

### Spot detection

HiTIPS includes morphologic, intensity, and filtering-based approaches for fluorescent spot detection. Currently, HiTIPS incorporates four different spot detection methods: Direct Thresholding, Gaussian Filter, Gaussian Laplacian, and Enhanced Gaussian Filter and Laplacian. The spot detection methods offered as part of HiTIPS have their own set of strengths and limitations, which need to be considered when choosing the appropriate spot detection method for a given type of biological sample and imaging assay.

The Direct Thresholding method applies a direct thresholding technique for spot segmentation without any filtering. It is a straightforward and computationally efficient approach suitable for scenarios where spots have large contrast. However, this method may be less effective when dealing with spots that have low contrast or are close to the background intensity level. Additionally, it has limited capability to handle spots with varying intensity gradients. The Gaussian Filter method utilizes a Gaussian filter to reduce noise and enhance spots. This method performs well when spots have a relatively uniform intensity distribution and works better when spots are close together or overlapping compared to the Gaussian Laplacian method. However, it may be less effective in enhancing spots with sharp intensity variations or irregular shapes. Careful consideration of parameters such as the Gaussian filter size ( $\sigma$ ) and thresholding parameters is necessary. The Gaussian Laplacian method enhances spots by applying a Gaussian Laplacian filter to the input image and then segments the spots using thresholding. By utilizing the negative lobes of the Gaussian Laplacian kernel, this method not only enhances the spots but also removes the background around the spot, improving the effectiveness of automatic thresholding. It is a relatively simple and computationally efficient method. However, it may face challenges when spots are closely located or overlapping due to limited resolution. Sensitivity to parameters such as the Laplacian filter size ( $\sigma$ ) and thresholding parameters should be considered. The Enhanced Gaussian Filter and Laplacian method, combines the strengths of both the Gaussian Filter and Gaussian Laplacian methods. It first applies a Gaussian filter to the input image, followed by a Gaussian Laplacian filter on the filtered image, and it finally uses fluorescence thresholding for spot segmentation. This method provides enhanced capabilities for detecting spots with varying intensity gradients and can improve overall spot detection accuracy. However, achieving optimal results may require careful tuning of filter sizes ( $\sigma$ ), and the choice of thresholding parameters may still impact its performance.

The spot detection methods provided in HiTIPS enable the detection and localization in the X and Y dimensions of fluorescent spots generated by DNA/RNA FISH staining, or from other biological structures in maximally projected 3D z-stacks microscopy images. Subsequently, maximum intensity or Gaussian-fitted maximum intensity can be employed to estimate the spot center positions in the Z dimension of the z-stack.

### Nuclei tracking

Nuclei tracking can be framed as a linear assignment problem in which  $N_i$  objects in frame  $i$  are matched up with  $N_{i+1}$  objects in frame  $i + 1$ . Shadow objects can be introduced to account for births (i.e. from cell division events) or deaths (i.e. cells leaving the field of view). We incorporated two cell tracking methods in HiTIPS to accommodate HTI assays using cell lines with different levels of confluency and mobility.

The first method we adopted<sup>56</sup> revisits and updates the Kalman filtering algorithm<sup>57</sup> and uses a Bayesian framework to improve the cell tracking accuracy and reliability. At the onset, the algorithm constructs tracklets, which are links between consecutive cell detections that do not exhibit cell division events. These tracklets from a prior frame are paired with observed cells in the current frame to form a Bayesian belief matrix, which initially holds a uniform probability of associations. Crucially, each tracklet deploys its own Kalman filter to predict the future state of a cell, basing its predictions on motion models and information from a cell state classifier. This classifier discerns nuclear morphological variations and chromatin condensation levels, which are crucial visual features in tracking. Belief updates in the matrix consider both motion evidence (using a constant velocity model) and appearance evidence (through a cell state transition matrix). The motion aspect focuses on the estimated

future position of a cell, while the appearance aspect evaluates linking probabilities based on the state transitions determined by the classifier. Notably, this combination method aids in accurately identifying instances like cell divisions. After forming these tracklets, a global optimization approach employing multiple hypothesis testing is used. It constructs a large number of hypotheses based on the appearance and motion features, with the aim of identifying the most optimal track-linking solution. Hypotheses account for diverse cell behaviors, including cell divisions, false-positive tracks, or apoptosis events. The optimal set of hypotheses is determined using a maximization function, resulting in the amalgamation of tracklets into final tracks. Ultimately, a graph-based approach is leveraged to assemble these tracks into lineage trees, outputting a set of additional measurements such as generational depth and cell lineage.

The second tracking method adopted by HiTIPS is DeepCell<sup>53,58</sup>. DeepCell employs a fully connected neural network that considers various features of each cell, including its appearance, local neighborhood, morphology, and motion. These pieces of information are fed into the neural network, which then processes and summarizes them into a vector representation using a deep learning sub-model. To determine the relationship between cells in consecutive frames, the information from the past frame and the current frame is utilized. The Hungarian algorithm<sup>59</sup> is employed for this purpose, which is a combinatorial optimization algorithm that assigns the best possible associations between cells across frames. It determines whether the current cell is the same as a cell in the previous frame, a different cell, or a child cell derived from the cell in the previous frame. By combining the DeepCell neural network with the Hungarian algorithm, this tracking method aims to accurately track and link cells across frames, considering their various characteristics and relationships.

### Nuclei/RNA spot image patch generation

Each cell track, representing the same nucleus monitored across the time-lapse movie, is precisely cropped from the full FOV into  $128 \times 128$  pixel image patches. At each time point, the cropping algorithm positions the center of mass of the segmented nucleus ROI at the center of the cropped image, thus optimizing the positioning and the orientation of the nuclei, which is further refined in the subsequent nucleus registration step. While it is possible to segment and track partial nuclei ROIs from the moment they enter the full FOV, until they partially exit it, this approach carries the risk of missing crucial objects or events in the nucleus. This can also potentially decrease the precision of frame-to-frame nuclei registration. Accordingly, HiTIPS provides the option to select only nuclei which are entirely within the frame, thereby improving the accuracy of tracking and RNA spot detection.

### Nuclei/RNA spots image patch registration

Accurate frame-to-frame rigid and rotational registration of the nucleus ROI is indispensable to track the dynamics of spots signals in the same nucleus over time. For example, in the time-lapse images of MS2/MCP-GFP labeled transcription sites, nuclei segmentation is often performed using the nucleoplasmic fluorescence background of the NLS-tagged MCP-GFP protein, which contains very little to no information about other sub-nuclear structures, such as nucleoli or chromocenters. As a consequence, feature-based image registration methods such as SIFT or SURF<sup>60–62</sup>, which rely on the presence of prominent texture features that remain consistent over time, cannot be utilized. To overcome this limitation, HiTIPS incorporates two novel registration methods that correct for nucleus translation and rotation across time-lapse movies. This is achieved by taking into account subtle variations in nuclear shape across the cropped ROI time-lapse movie in a two-step process (Supplementary Note 2, Algorithm 2 and Algorithm 3) that have been specifically designed for and implemented in HiTIPS. These methods provide an effective solution for tracking nuclei positioning across frames, thus facilitating the successful tracking of transcription sites in live cells.

The first method that we developed (Supplementary Note 2, Algorithm 2) starts with setting the angle between the major axis of the nucleus ( $\alpha$ ) and the horizon as zero. For each iteration greater than zero, two variables,  $\alpha'$  and  $\alpha''$ , are initialized at 0 and 180 degrees, respectively. The algorithm then computes eight specific features, namely, Cosine Similarity Index, Mutual Information, Structural Similarity Index, Mean Square Error, Variation of Information, Adaptive Random Error, and Peak Signal to Noise Ratio for these initial values of  $\alpha'$  and  $\alpha''$ . If the majority of the features for  $\alpha'$  exceed those for  $\alpha''$ , then the value of  $\alpha$  for this iteration is set as  $\alpha'$ , else it is set as  $\alpha''$ . This is followed by a process where  $\alpha'$  and  $\alpha''$  are set to  $\alpha \pm i$  (where  $i$  varies from 1 to 5) and a similar comparison of features is performed to update  $\alpha$ . The algorithm then increments the iteration count ( $n$ ), and repeats these steps until the final step, where the spot coordinates are mapped to the nuclei patch and used for spot tracking.

The second method that we developed (Supplementary Note 2, Algorithm 3) begins by assigning an initial rotation of 15 degrees to  $\alpha$  to prevent cumulative drift. Next, a series of transformations is performed on the centered nuclei including median filtering, upsampling, and polar warping. Following these transformations, sub-pixel image translation registration is carried out by cross-correlation in the polar Fourier domain. The algorithm then corrects for the initial rotation assigned in step one by subtracting it. The final step involves mapping the spot coordinates to the nuclei patch and tracking these spots using Algorithms 5 and 6 (Supplementary Note 2).

The intensity-based registration approach (Supplementary Note 2, Algorithm 2) has been proven to work better when cells shape changes during along the movement on their trajectory, however, large frame-to-frame intensity variations can introduce angle shift or translation in the registration results. On the other hand, the Fourier phase transform-based approach (Supplementary Note 2, Algorithm 3) is more robust to intensity change and less robust to frame-to-frame shape deformation.

### Assignment of transcription spots to timelapse tracks

The assignment of individual fluorescent spots detected at different time points to common tracks using hierarchical clustering integrates several algorithms for optimal results. We have developed a two-step process to effectively identify and organize spatial clusters of spots within each cell in projected stacks of images across the

time dimension. The first step (Supplementary Note 2, Algorithm 4) calculates the pairwise Euclidean distance between all transcription spots in the time-projected image, and then uses single-linkage hierarchical clustering to generate an initial set of labels for the clusters. This algorithm also identifies the centroids of each unique cluster label, it calculates the standard deviation of distances from the centroid for each cluster, and it identifies outlier spots that exceed a user-defined threshold distance from the centroid of the clusters. Once the outliers are identified they are arbitrarily labeled with a label of “zero”. The second algorithm (Supplementary Note 2, Algorithm 5) first determines the size of each cluster (i.e. the number of spots in the cluster) and separates them into “large” and “small” categories based on a user-defined threshold. Then, the algorithm calculates the Euclidean distances between points for each small cluster and all points in all the other large clusters. If the distance between the closest point in a large cluster is less than a user defined distance, the label of that closest point is assigned to the points in the small cluster. If not, it is labeled as an outlier. Through this process, small clusters and outliers are effectively merged into larger, more significant clusters, which streamlines the data structure and improves the interpretability of the results. The updated cluster labels, which correspond to tracks, for example of MS2/MCP-GFP representing sites of active gene transcription, across time, are then returned.

### Integrated intensity measurement

The integrated fluorescence intensity measurement of spots includes two components: Local background estimation and Gaussian mask fitting<sup>63</sup>. The Local Background Estimation Algorithm (Supplementary Note 2, Algorithm 6) first addresses the preprocessing of the images. This algorithm utilizes a least squares method to fit a background 2D plane using the fluorescence intensity values of the pixels at the border of an  $11 \times 11$  pixel matrix centered around the location of the spot. The estimated background plane is then subtracted from the original image, thus locally correcting for potential non-uniform illumination, and compensating for systematic imaging noise.

Following the background correction, the Gaussian Mask Fitting Algorithm (Supplementary Note 2, Algorithm 7) fits a Gaussian mask to the image to isolate and analyze individual spots within the image. The Gaussian mask can be either statically applied based on a given centroid or it can be iteratively adjusted to improve the accuracy of the fitting. The process involves iterative computation and adjustment of the centroid coordinates of the Gaussian mask until the difference between the old and new centroids becomes negligible, or until the maximum iteration count is reached. The final output from this process is the centroid coordinates of the Gaussian mask and the estimated photon number, which can then be used for further intensity track analysis.

### CENPC clustering score calculation

In our analysis, we employ a derivative of Ripley’s K-function<sup>32</sup>, specifically designed to estimate the degree of spatial clustering at the single-cell level. This statistical measure, denoted as  $K(r)$ , is defined as:

$$K(r) = \frac{A}{N(N-1)} \sum_{i \in \{C\}} \sum_{j \in \{C\}, j \neq i} I(d_{ij} < r)$$

In this equation,  $A$  represents the nucleus area for each cell,  $N$  is the total number of CENPC spots in the nucleus,  $d_{ij}$  stands for the Euclidean distance between the  $i$ -th and  $j$ -th spots, and  $r$  is a predefined radius within which we evaluate the clustering. The indicator function,  $I()$ , returns 1 if  $(d_{ij} < r)$ , and 0 otherwise. The calculation of  $K(r)$  involves the summation over all unique pairs of points  $(i, j)$  in the cell  $(C)$ . The resulting sum is then normalized by multiplying it to the ratio between  $A$  and the product of  $N$  and  $N-1$ .

To correct for edge effects, which can potentially bias results for spots in proximity of the nucleus ROI periphery, we employ Ripley’s edge-corrected K-function. The correction to the K-function adds a weighting term for each point that is inversely proportional to the area of the region accessible to other points within the specified radius,  $r$ , without crossing the boundary of the study area. This results in a correction factor that adjusts for the reduced probability of finding neighboring points near the edges of the region under study. The  $K(r)$  calculations were performed using the Astropy package in a Jupyter notebook separate from HiTIPS. Finally, the difference between a Poisson point process (representing complete spatial randomness) and the actual data from the cell is computed. The percentage of radii where the measured value of  $K(r)$  is higher than the  $K(r)$  for the Poisson process is then calculated as a clustering score on a per cell basis.

### Statistical analysis

Statistical analysis for the DNA FISH and for the CENPC clustering data was performed using the R statistical programming language, and these R packages: tidyverse, data.table, fs, and ggthemes.

Statistical analysis for the MS2-GFP live cell data was performed in Python 3.9 using these libraries: pandas, Seaborn and Matplotlib.

### Data availability

The original imaging metadata generated by our high-throughput microscopes follow most of the QUAREP-LIMI guidelines<sup>64,65</sup> and includes all the microscope and imaging settings used to acquire the data. In addition, we have also generated a additional set of image acquisition metadata in the QUAREP-LIMI json format using the Micro-Meta App<sup>66</sup>. All the images and the image acquisition metadata used in the manuscript have been deposited at BioImage Archive<sup>67</sup> under accession number S-BIAD1043 at: <https://www.ebi.ac.uk/biostudies/BioImages/studies/S-BIAD1043>.

## Code availability

The HiTIPS code base can be found at <https://github.com/CBIIT/HiTIPS>. A complete guide describing the HiTIPS package structure and its embedded functions, installation and user instruction, results tables description, and developers guide to add new analysis methods is available at <https://hitips.readthedocs.io/en/latest/>.

Received: 27 October 2023; Accepted: 2 July 2024

Published online: 08 August 2024

## References

- Boutros, M., Heigwer, F. & Laufer, C. Microscopy-based high-content screening. *Cell* **163**, 1314–1325 (2015).
- Pegoraro, G. & Misteli, T. High-throughput imaging for the discovery of cellular mechanisms of disease. *Trends Genet.* **33**, 604–615 (2017).
- Joyce, E. F., Williams, B. R., Xie, T. & Wu, C.-T. Identification of genes that promote or antagonize somatic homolog pairing using a high-throughput FISH-based screen. *PLoS Genet.* **8**, e1002667 (2012).
- Shachar, S., Voss, T. C., Pegoraro, G., Sciascia, N. & Misteli, T. Identification of gene positioning factors using high-throughput imaging mapping. *Cell* **162**, 911–923 (2015).
- Jowhar, Z. *et al.* Effects of human sex chromosome dosage on spatial chromosome organization. *Mol. Biol. Cell* **29**, 2458–2469 (2018).
- Finn, E. H. *et al.* Extensive heterogeneity and intrinsic variation in spatial genome organization. *Cell* **176**, 1502–1515.e10 (2019).
- Park, D. S. *et al.* High-throughput Oligopaint screen identifies druggable 3D genome regulators. *Nature* <https://doi.org/10.1038/s41586-023-06340-w> (2023).
- Neumann, B. *et al.* Phenotypic profiling of the human genome by time-lapse microscopy reveals cell division genes. *Nature* **464**, 721–727 (2010).
- Cuylen, S. *et al.* Ki-67 acts as a biological surfactant to disperse mitotic chromosomes. *Nature* **535**, 308–312 (2016).
- Kubben, N. *et al.* Repression of the antioxidant NRF2 pathway in premature aging. *Cell* **165**, 1361–1374 (2016).
- Samwer, M. *et al.* DNA cross-bridging shapes a single nucleus from a set of mitotic chromosomes. *Cell* **170**, 956–972.e23 (2017).
- Jevtić, P. *et al.* The nucleoporin ELYS regulates nuclear size by controlling NPC number and nuclear import capacity. *EMBO Rep.* **20**, (2019).
- Schibler, A. C., Jevtic, P., Pegoraro, G., Levy, D. L. & Misteli, T. Identification of epigenetic modulators as determinants of nuclear size and shape. *Elife* **12**, (2023).
- Stavreva, D. A. *et al.* Transcriptional bursting and co-bursting regulation by steroid hormone release pattern and transcription factor mobility. *Mol. Cell* **75**, 1161–1177.e11 (2019).
- Wan, Y. *et al.* Dynamic imaging of nascent RNA reveals general principles of transcription dynamics and stochastic splice site selection. *Cell* **184**, 2878–2895.e20 (2021).
- Ljosa, V. & Carpenter, A. E. Introduction to the quantitative analysis of two-dimensional fluorescence microscopy images for cell-based screening. *PLoS Comput. Biol.* **5**, e1000603 (2009).
- Imbert, A. *et al.* FISH-quant v2: A scalable and modular tool for smFISH image analysis. *RNA N. Y. N* **28**, 786–795 (2022).
- Carpenter, A. E. *et al.* Cell Profiler: Image analysis software for identifying and quantifying cell phenotypes. *Genome Biol.* **7**, R100 (2006).
- Stirling, D. R. *et al.* Cell Profiler 4: Improvements in speed, utility and usability. *BMC Bioinform.* **22**, 433 (2021).
- Linkert, M. *et al.* Metadata matters: Access to image data in the real world. *J. Cell Biol.* **189**, 777–782 (2010).
- Edelstein, A., Amodaj, N., Hoover, K., Vale, R. & Stuurman, N. Computer control of microscopes using µManager. *Curr. Protoc. Mol. Biol.* Chapter 14, Unit14.20 (2010).
- Moore, J. *et al.* OME-Zarr: A cloud-optimized bioimaging file format with international community support. *bioRxiv* 2023.02.17.528834 (2023).
- Misteli, T. The self-organizing genome: Principles of genome architecture and function. *Cell* **183**, 28–45 (2020).
- Lieberman-Aiden, E. *et al.* Comprehensive mapping of long-range interactions reveals folding principles of the human genome. *Science* **326**, 289–293 (2009).
- Rao, S. S. P. *et al.* Cohesin loss eliminates all loop domains. *Cell* **171**, 305–320.e24 (2017).
- Luppino, J. M. *et al.* Cohesin promotes stochastic domain intermingling to ensure proper regulation of boundary-proximal genes. *Nat. Genet.* **52**, 840–848 (2020).
- Natsume, T., Kiyomitsu, T., Saga, Y. & Kanemaki, M. T. Rapid protein depletion in human cells by auxin-inducible degron tagging with short homology donors. *Cell Rep* **15**, 210–218 (2016).
- Przewłoka, M. R. *et al.* CENP-C is a structural platform for kinetochore assembly. *Curr. Biol. CB* **21**, 399–405 (2011).
- Foley, E. A. & Kapoor, T. M. Microtubule attachment and spindle assembly checkpoint signalling at the kinetochore. *Nat. Rev. Mol. Cell Biol.* **14**, 25–37 (2013).
- Muller, H., Gil, J. & Drinnenberg, I. A. The impact of centromeres on spatial genome architecture. *Trends Genet. TIG* **35**, 565–578 (2019).
- Hoencamp, C. *et al.* 3D genomics across the tree of life reveals condensin II as a determinant of architecture type. *Science* **372**, 984–989 (2021).
- Kiskowski, M. A., Hancock, J. F. & Kenworthy, A. K. On the use of Ripley's K-function and its derivatives to analyze domain size. *Biophys. J.* **97**, 1095–1103 (2009).
- Rodriguez, J. *et al.* Intrinsic dynamics of a human gene reveal the basis of expression heterogeneity. *Cell* **176**, 213–226.e18 (2019).
- Schneider, C. A., Rasband, W. S. & Eliceiri, K. W. NIH Image to ImageJ: 25 years of Image analysis. *Nat. Methods* **9**, 671–675 (2012).
- Ahlers, J. *et al.* napari: A multi-dimensional image viewer for Python. *Zenodo* <https://doi.org/10.5281/zenodo.8115575> (2023).
- Pape, C. *et al.* MoBIE: A Fiji plugin for sharing and exploration of multi-modal cloud-hosted big image data. *Nat. Methods* **20**, 475–476 (2023).
- Barry, D. J., Gerri, C., Bell, D. M., D'Antuono, R. & Niakan, K. K. GIANI—Open-source software for automated analysis of 3D microscopy images. *J. Cell Sci.* **135**, 259511 (2022).
- Ritchie, A., Laitinen, S., Katajisto, P. & Englund, J. I. “Tonga”: A novel toolbox for straightforward bioimage analysis. *Front. Comput. Sci.* **4**, (2022).
- Fillbrunn, A. *et al.* KNIME for reproducible cross-domain analysis of life science data. *J. Biotechnol.* **261**, 149–156 (2017).
- Dietz, C. & Berthold, M. R. KNIME for open-source bioimage analysis: A tutorial. *Adv. Anat. Embryol. Cell Biol.* **219**, 179–197 (2016).
- Gudla, P. R., Nakayama, K., Pegoraro, G. & Misteli, T. SpotLearn: Convolutional neural network for detection of fluorescence in situ hybridization (FISH) signals in high-throughput imaging approaches. *Cold Spring Harb. Symp. Quant. Biol.* **82**, 57–70 (2017).
- Zaki, G. *et al.* A deep learning pipeline for nucleus segmentation. *Cytom. A* **97**, 1248–1264 (2020).
- Savulescu, A. F. *et al.* Interrogating RNA and protein spatial subcellular distribution in smFISH data with DypFISH. *Cell Rep. Methods* **1**, 100068 (2021).

44. Bahry, E. *et al.* RS-FISH: Precise, interactive, fast, and scalable FISH spot detection. *Nat. Methods* **19**, 1563–1567 (2022).
45. Ouyang, W., Mueller, F., Hjelmare, M., Lundberg, E. & Zimmer, C. ImJoy: An open-source computational platform for the deep learning era. *Nat. Methods* **16**, 1199–1200 (2019).
46. Hart, T. *et al.* High-resolution CRISPR screens reveal fitness genes and genotype-specific cancer liabilities. *Cell* **163**, 1515–1526 (2015).
47. Finn, E., Misteli, T. & Pegoraro, G. High-throughput DNA FISH (hiFISH). *Methods Mol. Biol.* **2532**, 245–274 (2022).
48. Coulon, A. *et al.* Kinetic competition during the transcription cycle results in stochastic RNA processing. *Elife* **3**, (2014).
49. Bannon, D. *et al.* DeepCell 2.0: Automated cloud deployment of deep learning models for large-scale cellular image analysis. Preprint at <https://doi.org/10.1101/505032> (2018).
50. Stringer, C., Wang, T., Michaelos, M. & Pachitariu, M. Cellpose: a generalist algorithm for cellular segmentation. *Nat. Methods* **18**, 100–106 (2021).
51. Hollandi, R. *et al.* Nucleus segmentation: Towards automated solutions. *Trends Cell Biol.* **32**, 295–310 (2022).
52. Pachitariu, M. & Stringer, C. Cellpose 2.0: How to train your own model. *Nat. Methods* **19**, 1634–1641 (2022).
53. Greenwald, N. F. *et al.* Whole-cell segmentation of tissue images with human-level performance using large-scale data annotation and deep learning. *Nat. Biotechnol.* **40**, 555–565 (2022).
54. Yang, X., Li, H. & Zhou, X. Nuclei segmentation using marker-controlled watershed, tracking using mean-shift, and Kalman filter in time-lapse microscopy. *IEEE Trans. Circuits Syst. Regul. Pap.* **53**, 2405–2414 (2006).
55. Soille, P. *Morphological Image Analysis* (Springer, 2004). <https://doi.org/10.1007/978-3-662-05088-0>.
56. Ulicna, K., Vallardi, G., Charras, G. & Lowe, A. R. Automated deep lineage tree analysis using a Bayesian single cell tracking approach. *Front. Comput. Sci.* **3**, (2021).
57. Kalman, R. E. A new approach to linear filtering and prediction problems. *J. Basic Eng.* **82**, 35–45 (1960).
58. Moen, E. *et al.* Accurate cell tracking and lineage construction in live-cell imaging experiments with deep learning. Preprint at <https://doi.org/10.1101/803205> (2019).
59. Kuhn, H. W. The Hungarian method for the assignment problem. *Nav. Res. Logist. Q.* **2**, 83–97 (1955).
60. Lowe, D. G. Distinctive image features from scale-invariant keypoints. *Int. J. Comput. Vis.* **60**, 91–110 (2004).
61. Bay, H., Ess, A., Tuytelaars, T. & Van Gool, L. Speeded-up robust features (SURF). *Comput. Vis. Image Underst.* **110**, 346–359 (2008).
62. Ma, W. *et al.* Remote sensing image registration with modified SIFT and enhanced feature matching. *IEEE Geosci. Remote Sens. Lett.* **14**, 3–7 (2017).
63. Thompson, R. E., Larson, D. R. & Webb, W. W. Precise nanometer localization analysis for individual fluorescent probes. *Biophys. J.* **82**, 2775–2783 (2002).
64. Nelson, G. *et al.* QUAREP-LiMi: A community-driven initiative to establish guidelines for quality assessment and reproducibility for instruments and images in light microscopy. *J. Microsc.* **284**, 56–73 (2021).
65. Hammer, M. *et al.* Towards community-driven metadata standards for light microscopy: Tiered specifications extending the OME model. *Nat. Methods* **18**, 1427–1440 (2021).
66. Rigano, A. *et al.* Micro-Meta App: An interactive tool for collecting microscopy metadata based on community specifications. *Nat. Methods* **18**, 1489–1495 (2021).
67. Hartley, M. *et al.* The bioimage archive—Building a home for life-sciences microscopy data. *J. Mol. Biol.* **434**, 167505 (2022).

## Acknowledgements

We would like to thank all the members of the Misteli and Larson laboratories for insightful discussions on high-throughput imaging and automated image analysis. This work utilized the computational resources of the NIH HPC Biowulf cluster (<http://hpc.nih.gov>). We would like to thank the NIH HPC group for their help with data management and software package management. Finally, we would also like to thank the anonymous reviewers for their constructive criticism and feedback for our work, which have substantially improved the original version of the manuscript. Research in the Misteli Lab, Larson Lab, and HiTIF was supported by the Intramural Research Program of the NIH, NCI, Center for Cancer Research via 1-ZIA-BC010309-24, 1-ZIA-BC011383-12, and 1-ZIC-BC011567-09, respectively.

## Author contributions

A.K. and G.P. established the requirements for HiTIPS. A.K. wrote all the HiTIPS code base. F.A., K.G., and V.S. performed cell culture and treated cells for DNA FISH, IF, and live cell imaging, respectively. F.A., K.G., and V.S. acquired the images with high-throughput microscopes. A.K., F.A., and K.G. analyzed the high-throughput imaging datasets using HiTIPS and performed statistical analysis and plotting. A.K., F.A., K.G., V.S., N.F., C.H.B., D.R.L., and T.M., and G.P. provided guidance and feedback on the algorithms for image analysis and on the design of the graphical user interface. A.K. and G.P. wrote the manuscript. All authors edited and approved the manuscript.

## Funding

Open access funding provided by the National Institutes of Health.

## Competing interests

The authors declare no competing interests.

## Additional information

**Supplementary Information** The online version contains supplementary material available at <https://doi.org/10.1038/s41598-024-66600-1>.

**Correspondence** and requests for materials should be addressed to G.P.

**Reprints and permissions information** is available at [www.nature.com/reprints](http://www.nature.com/reprints).

**Publisher's note** Springer Nature remains neutral with regard to jurisdictional claims in published maps and institutional affiliations.

**Open Access** This article is licensed under a Creative Commons Attribution 4.0 International License, which permits use, sharing, adaptation, distribution and reproduction in any medium or format, as long as you give appropriate credit to the original author(s) and the source, provide a link to the Creative Commons licence, and indicate if changes were made. The images or other third party material in this article are included in the article's Creative Commons licence, unless indicated otherwise in a credit line to the material. If material is not included in the article's Creative Commons licence and your intended use is not permitted by statutory regulation or exceeds the permitted use, you will need to obtain permission directly from the copyright holder. To view a copy of this licence, visit <http://creativecommons.org/licenses/by/4.0/>.

This is a U.S. Government work and not under copyright protection in the US; foreign copyright protection may apply 2024